Shock Waves in Gas-Particle Mixtures

By

Ryuji ISHII*

(Received January 21, 1983)

Abstract

Shock waves in a dusty gas are analyzed numerically by taking into account a continuous distribution of particle sizes. A distribution function for the particle radii is introduced in order to describe the continuous particle sizes. The equations for the gas and the particles are solved by the Runge-Kutta-Gill method, where the integrations in these equations are calculated with Simpson's formula. It is made clear that the effects on the flow, or the flow structure, behind a shock front of the distribution function are very important. Also, the usual approximation for single sizes of particles will lead to poor results in many practical problems.

Introduction

Shock waves in a mixture of a gas and small solid particles are analyzed numerically. There have been many works treating shock waves in a dusty gas[1]-[9]. Most of them are, however, concerned with flows having a single uniform size of particles. Only a few works are concerned with a few distinct sizes of particles[9]. In many practical cases, it may not be natural nor reasonable to consider that all the particles have a single uniform size. Even when the particle sizes are approximated by a few distinct representative sizes, the validity or the accuracy of the approximation could not be assessed without the results of a more general or exact analysis. The accuracy of the few-sizes approximation may be dependent upon the actual form of the size distribution of particles. In any case, at least theoretically, it may be preferable to consider the continuous distribution of particle sizes in order to predict the flow behavior of the gas-particle mixture with sufficient accuracy and generality.

Here, the shock waves in a dusty gas are treated by assuming that the particles have a continuous distribution of sizes. A distribution function for the particle radii is introduced in order to take into account the continuous distribution of particle sizes. The one-dimensional stationary flow is considered, its direction being identical with the direction of the positive x-direction. The mixture is assumed to be in a constant

* Department of Aeronautical Engineering.

state of equilibrium far upstream, and the particle volume fraction is assumed to be negligibly small. Although the last assumption is not always essentially necessary in the present analysis, it is introduced primarily for simplicity.

Basic Equations

The dimension-less quantities are introduced by

$$x = \frac{\bar{x}}{\bar{L}}, \quad V = \frac{\bar{V}}{\bar{V}_0}, \quad \rho = \frac{\bar{\rho}}{\bar{\rho}_0}, \quad p = \frac{\bar{p}}{\bar{p}_0}, \quad T = \frac{\bar{T}}{\bar{T}_0},$$

$$V_p = \frac{\bar{V}_p}{\bar{V}_0}, \quad \rho_p = \frac{\bar{\rho}_p}{\bar{\rho}_{p0}}, \quad n_p = \frac{\bar{n}_p}{\bar{n}_{p0}}, \quad T_p = \frac{\bar{T}_p}{\bar{T}_0},$$

$$r_p = \frac{\bar{r}_p}{\bar{l}_p}, \quad \phi = \bar{l}_p \bar{\phi}, \tag{1}$$

where $\bar{x}$ is the distance measured from a shock front, and $\bar{\rho}$, $\bar{V}$, $\bar{p}$, and $\bar{T}$ are the density, the velocity, the pressure, and the temperature of the gas, respectively. The quantities associated with the solid particles are designated by the subscript p. The quantities $\bar{n}_p$, $\bar{r}_p$, and $\bar{\phi}$ are the number density, the radius and the distribution function of the sizes of the solid particles. The constants $\bar{L}$ and $\bar{l}_p$ are the reference length behind the shock front and the reference particle radius. The subscript zero designates the upstream equilibrium conditions. Under the upstream equilibrim conditions, it can be assumed that $\bar{V}_0 = \bar{V}_{p0}$ and $\bar{T}_0 = \bar{T}_{p0}$.

The particle density $\bar{\rho}_p$ is related to $\bar{n}_p$ by

$$\bar{\rho}_p = \frac{4}{3} \pi \bar{\rho}_{mp} \bar{n}_p \int_{\bar{r}_{pmin}}^{\bar{r}_{pmax}} \bar{\phi} \bar{r}_p^3 d\bar{r}_p, \tag{2}$$

where $\bar{\rho}_{mp}$ is the material density of the solid particles, and $\bar{r}_{pmax}$ and $\bar{r}_{pmin}$ are the maximum and the minimum radii of the particles contained in the flow. The distribution function is generally a function of $\bar{r}_p$ as well as $\bar{x}$, and is defined such that the number of particles which have radii $\bar{r}_p$ lying $\bar{r}_p$ to $\bar{r}_p + d\bar{r}_p$ is

$$\bar{n}_p \bar{\phi} \, d\bar{r}_p,$$

per unit volume, This satisfies the next normalizing condition :

$$\int_{\bar{r}_{pmin}}^{\bar{r}_{pmax}} \bar{\phi} \, d\bar{r}_p = 1. \tag{3}$$

Here, attention must be paid to the fact that the number density $\bar{n}_p$ is independent of $\bar{r}_p$, and is only a function of $\bar{x}$.

Introducing the additional usual assumptions, the one-dimensional flow of the dusty gas may be written with the dimension-less quantities introduced in Eq. (1) as follows :

$$\rho V = 1, \tag{4}$$

$$V + \frac{p}{\gamma M_0^2} + \nu \int_a^b \phi_0 V_p r_p^3 dr_p = 1 + \frac{1}{\gamma M_0^2} + \nu \int_a^b \phi_0 r_p^3 dr_p, \tag{5}$$

$$T + \frac{\gamma-1}{2}M_0^2 V^2 + \nu \int_a^b \phi_0 \left(\theta T_p + \frac{\gamma-1}{2}M_0^2 V_p^2\right) r_p^3 \, dr_p$$

$$= 1 + \frac{\gamma-1}{2}M_0^2 + \nu\left(\theta + \frac{\gamma-1}{2}M_0^2\right)\int_a^b \phi_0 r_p^3 \, dr_p, \tag{6}$$

$$p = \rho T, \tag{7}$$

$$n_p \phi V_p = \phi_0, \tag{8}$$

(See Appendix)

$$n_p = \int_a^b \frac{\phi_0}{V_p} dr_p, \tag{9}$$

$$V_p \frac{dV_p}{dx} = A_{p0} f_p \frac{T^\alpha}{r_p^2}(V - V_p), \tag{10}$$

$$V_p \frac{dT_p}{dx} = \lambda A_{p0} g_p \frac{T^\alpha}{r_p^2}(T - T_p), \tag{11}$$

where

$$\nu = \frac{4}{3}\pi \bar{l}_p^3 \bar{\rho}_{mp} \frac{\bar{n}_{p0}}{\rho_0}, \tag{12}$$

$$A_{p0} = \frac{9}{2}\frac{\bar{\mu}_0}{\bar{\rho}_{mp}\bar{l}_p^2}\frac{\bar{L}}{\bar{V}_0}, \tag{13}$$

$$M_0^2 = \bar{V}_0^2 / \left(\gamma \frac{\bar{p}_0}{\bar{\rho}_0}\right), \tag{14}$$

$$\theta = \bar{C}_{pp}/\bar{C}_{pg}, \tag{15}$$

$$\lambda = 2\bar{C}_{pg}/(3P_r\bar{C}_{pp}), \tag{16}$$

$$f_p = C_D/C_{D stokes}, \quad g_p = N_u/N_{ustokes}, \tag{17}$$

$$a = \bar{r}_{pmin}/\bar{l}_p, \quad b = \bar{r}_{pmax}/\bar{l}_p. \tag{18}$$

Here, the normalizing condition for the distribution function is rewritten in the non-dimensional form:

$$\int_a^b \phi \, dr_p = 1, \tag{19}$$

which was used in deriving Eq. (9) from Eq. (8). In Eqs. (4) to (18), M is the Mach number for the gas flow, and the parameters P_r, C_D, and N_u are the Prandtle number, the drag coefficient, and the Nusselt number, respectively. The subscript Stokes denotes the values evaluated in Stokes' theory. The constants $\bar{C}_{pg}$ and $\bar{C}_{pp}$ are the specific heat at the constant pressure of the gas and the specific heat of the solid material. The ratio of the specific heats of the gas is denoted by γ. The coefficient of the viscosity of the gas $\bar{\mu}$ is assumed here to be

$$\bar{\mu} \propto \bar{T}^{\alpha}. \tag{20}$$

In Eq. (20), α is a constant to be specified properly according to the particular problem. Here, it is chosen to be 0.6. The system of eight equations, (4) to (11), is sufficient to determine the eight variables ρ, V, T, p, V_p, n_p, T_p, and ϕ. It must be noted that V_p, T_p, and ϕ are here the functions of r_p as well as x. Eqs. (10) and (11) are the momentum and energy equations of a single particle having a radius r_p.

At this point, it is necessary to specify the reference lengths l_p and $\bar{L}$. One reasonable choice of l_p may be given by l_{p0} which satisfies

$$\frac{4}{3}\pi\bar{\rho}_{mp}l_p^3\bar{n}_{p0}, \ =\bar{\rho}_{p0},$$

where $\bar{\rho}_p$ is given by Eq. (2). This can be rewritten as

$$l_{p0}^3 = \int_{\bar{r}_{pmin}}^{\bar{r}_{pmax}} \bar{\phi}_0 \bar{r}_p^3 d\bar{r}_p. \tag{21}$$

This value of $\bar{l}_{p0}$ corresponds to the radius of particles having an average mass over all sizes of particles. In this case, the value of ν in Eq. (12) yields the mass flow ratio of the solid particles to the gas.

In the numerical calculations, however, such a choice of $\bar{l}_{p0}$ as a reference radius is not always convenient. Here, therefore, $\bar{l}_p$ is chosen next :

$$l_p = \bar{r}_{pmin}, \tag{22}$$

which yields

$$a = 1, \quad b = \bar{r}_{pmax}/\bar{r}_{pmin}. \tag{23}$$

In this case the mass flow ratio ζ is given by

$$\zeta = \nu n_p \int_1^b V_p \phi r_p^3 dr_p = \nu \int_1^b \phi_0 r_p^3 dr_p. \tag{24}$$

The choice of $\bar{l}_p$, as in Eq. (22), is convenient in the numerical integration of Eqs (10) and (12), because the most difficult situation usually happens for the smallest sizes of particles.

Another remaining reference length L is specified as

$$A_{p0} = \frac{9}{2} \frac{\bar{\mu}_0}{\bar{\rho}_{mp}\bar{l}_p^2} \frac{\bar{L}}{\bar{V}_0} = 1. \tag{25}$$

As was stated proviously, such a choice of the reference lengths have been made mainly for numerical convenience. It will be easy to realize that in this case the whole relaxation region may be measured roughly by $\bar{L}_{max}$,

$$\bar{L}_{max} = \bar{L}b^2/[T_i^\alpha(f_{pi})_{r_p=b}], \tag{26}$$

where the subscript s denotes the conditions just behind the shock front. This is because the largest sizes of particles have the largest relaxation length and the magnitudes of f_p and g_p in Eqs. (10) and (11) are usually of the same order. This value of $\bar{L}_{max}$ is, however, not always reliable for use in estimating the effective relaxation length, since different sizes of particles have different relaxation lengths. Then, it will be more reasonable and convenient to take the next value $\bar{L}_e$ as an effective relaxation length:

$$\bar{L}_e = \bar{L}r_{ps}^2 / [T_s^\alpha (f_{ps})_{r_p=r_{ps}}], \tag{27}$$

where $r_{ps} = \bar{l}_{p0}/\bar{r}_{p\,min}$. It will be easy to see that $\bar{L}_e$, defined by Eq. (27), is the relaxation length corresponding to the particles with the average radius $\bar{l}_{p0}$ given in Eq. (22).

Assuming that the particle sizes are negligibly small compared with the relaxation lengths, we can write the boundary conditions at (just behind) the shock front to the system as follows:

$$V_s = \left(1 + \frac{\gamma-1}{2}M_0^2\right) \bigg/ \left(\frac{\gamma+1}{2}M_0^2\right),$$

$$T_s = \left(1 + \frac{\gamma-1}{2}M_0^2\right)\left(\gamma M_0^2 - \frac{\gamma-1}{2}\right) \bigg/ \left[\frac{1}{4}(\gamma+1)^2 M_0^2\right], \tag{28}$$

$$\phi_s = \phi_0,$$
$$V_{ps} = 1, \tag{29}$$
$$T_{ps} = 1.$$

Now, it must be noticed that ϕ, V_p, and T_p in the basic equations are functions of r_p and x (ρ, V, p, T, and n_p are functions of x only).

Numerical Analysis

A. Numerical Scheme

To carry out the analysis, it is necessary to give f_p and g_p in Eq. (17). In the present analysis, the equation by Henderson in Ref. 10 and that by Carlson and Hoglund in Ref. 11 are used for f_p and g_p, respectively.

One major difficulty in the numerical analysis occurs in connection with the integrations over r_p in Eqs. (5), (6), and (9). This difficulty is overcome by employing the usual numerical approximation, Simpson's formula:

$$\int_1^b F(r_p,\ x)\,dr_p \approx \sum_{k=1}^{(n-1)/2} \frac{H}{3}(F_{2k-1} + 4F_{2k} + F_{2k+1}), \tag{30}$$

where

$$H = \frac{b-1}{n-1},$$
$$F_i = F(r_{pi},\ x),$$

$$r_{pi} = 1 + (i-1)H.$$

In Eq. (30), $F(r_p, x)$ is any function of r_p and x, and n, k, and i are an odd number greater than 2, an integer in the range $1 \leq k \leq (n-1)/2$, and an integer in the range $1 \leq i \leq n$, respectively.

According to the approximation (30), there are the n sets of equations :

$$n_p \phi_i V_{pi} = \phi_{0i},$$ (31)

$$V_{pi} \frac{dV_{pi}}{dx} = f_{pi} \frac{T^\alpha}{r_{pi}^2} (V - V_{pi}),$$ (32)

$$V_{pi} \frac{dT_{pi}}{dx} = \lambda g_{pi} \frac{T^\alpha}{r_{pi}^2} (T - T_{pi}),$$ (33)

where $i = 1, 2, 3, \cdots, n$. These are considered in place of Eqs. (8), (10), and (11). Then, numerically, the problem is reduced to solving these n sets of equations (31) to (33) in conjunction with Eqs. (4) to (7), and Eq. (9), where the boundary conditions for ϕ, V_p and T_p in Eq. (29) are rewritten as

$$\phi_{is} = \phi_{0i},$$
$$V_{pis} = 1,$$ (34)
$$T_{pis} = 1.$$

Mathematically, in the present analysis, the relaxation equations (10) and (11), which are for a particle with every radius r_p, are replaced by the n sets of equations, Eqs. (32) and (33), for n representative sizes of particles. The effect of the interactions between the gas and all sizes of particles on the gas flow is taken into account through the integral terms over all sizes of particles in Eqs. (5) and (6). These are calculated numerically by Simpson's formula (30) with the particle velocities V_{pi}, temperatures T_{pi}, and the distribution functions ϕ_i of the n representative sizes of particles.

In the numerical integration of the system with respect to x, the fourth-order Runge-Kutta-Gill method is applied in conjunction with the approximations, Eq. (30), to the integral terms in Eqs. (5), (6) and (9). Since the quantities λ and g_p/f_p are usually of an order unity, the mesh size Δx is reasonably chosen so as to satisfy

$$\Delta x \ll 1/[T_s^\alpha (f_{pi})_{r_p=1}],$$

in order to stabilize the numerical integration with respect to the distance x.

B. Sample calculations

For sample calculations, we consider a flow with small solid particles of Al_2O_3 which are produced, for example, in the combustion process in the rocket motors with a solid propellant. The physical constants used in the present calculation are listed in Table 1.

Table 1. Physical constants

$\gamma = 1.29$	
$\bar{C}_{pg} = 2008.0$ J/kg. °K	
$P_r = 0.75$	
$\bar{\mu} = 2.6 \times 10^{-5}$ kg/sec m (for 300°K)	
$\alpha = 0.6$	
$\bar{C}_{pp} = 1686.0$ J/kg °K	
$\bar{\rho}_{mp} = 4.0 \times 10^3$ kg/m³	

At this stage, one remaining task is to specify the initial distribution function $\phi_0 = \phi_0(r_p)$ for the particle radii. Practically, however, it is very difficult to specify it, and at least up to now, there has been little data for the size distribution of Al_2O_3. Here, therefore, we consider the function ϕ_0 in the form,

$$\phi_0 = Cr_p^c \exp(-Dr_p^d),$$

where D, c, and d are the constants specified properly, and the constant C is to be determined for these specified values of D, c, and d from the normalizing condition, Eq. (19). In the present analysis, two sets of values are considered :

Case (a)

$$C = 84.322, \quad c = -5,$$
$$D = 6.4, \quad d = -2,$$

Case (b)

$$C = 0.14286, \quad c = 0,$$
$$D = 0, \quad d = 0.$$

The minimum and the maximum particle radii, $\bar{r}_{pmin}$ and $\bar{r}_{pmax}$, are specified as follows,

$$\bar{r}_{pmin} = 0.5\mu,$$
$$\bar{r}_{pmax} = 4.0\mu.$$

The non-dimensional maximum radius b in Eq. (23) is now determined to be 8. The first set of values in Case (a) is determined from the experimental results in Ref. 4 by a curve fitting. The latter set of values in Case (b) is only a fictitious uniform distribution. It must be noticed that the value of D in Case (a) depends on the dimensional value of $\bar{r}_{pmin}(=\bar{l}_p)$. The functions ϕ_0 and $r_p^3\phi_0$ are plotted against r_p in Figs. 1 and 2. The latter quantity is very important, because the magnitude of the effect on the gas flow of the particles with radii r_p lying r_p to $r_p + dr_p$ due to the interactions between them is more directly related to their masses ($\propto r_p^3\phi dr_p$) than to the number ($\propto \phi dr_p$) itself.

The upstream equilibrium conditions in the dimensional form are specified as follows :

$$\bar{\rho}_0 = 0.1 \ kg/m^3,$$
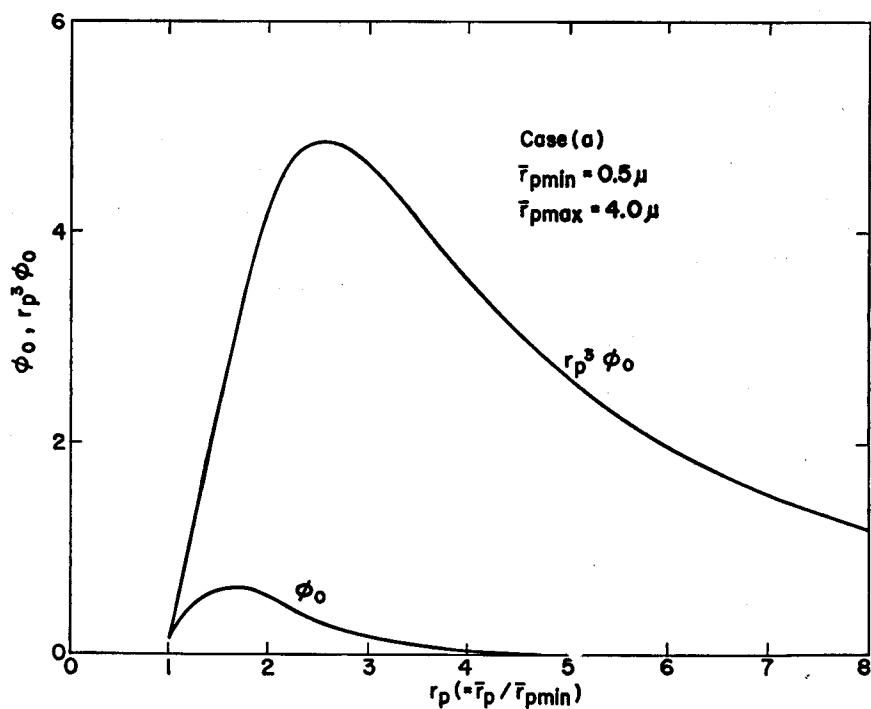$$\bar{V}_0 = 1.254 \times 10^3 \ m/sec,$$

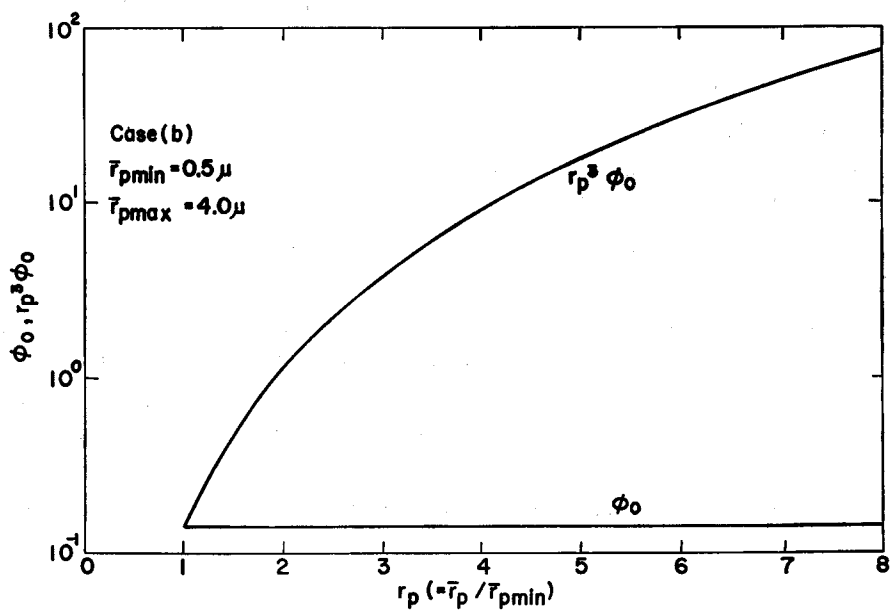Fig. 1. Functions $\phi_0(r_p)$ and $r_p^3\phi_0(r_p)$ for Case (a).

Fig. 2. Functions $\phi_0(r_p)$ and $r_p^3\phi_0(r_p)$ for Case (b).

$$\bar{T}_0 = 300^\circ K,$$

$$\bar{p}_0 = 1.354 \times 10^4 \quad N/m = 0.1336\ atm,$$

$$M_0 = 3,$$

$$\zeta = 0.3.$$

Under these conditions, the shock conditions can be determined and non-dimensionalized as follows,

$$\rho_s = 4.471,$$

$$V_s = 0.2237,$$

$$T_s = 2.240,$$

$$p_s = 10.01,$$

at (just behind) the shock front $(x = 0)$, and

$$\rho = n_p = 5.833,$$

$$V = V_p = 0.1714,$$

$$T = T_p = 2.315,$$

$$p = 13.51,$$

far downstream of the front $(x = \infty)$. The shock conditions at $x = \infty$ given above have been calculated from the usual shock relations under the equilibrium conditions $\rho = n_p$, $V = V_p$, $T = T_p$, and $\phi = \phi_0$ in Eqs. (4-9).

The average radii $_{p0}$ for Cases (a) and (b) are calculated from Eq. (21) to yield

$$l_{p0} = \begin{cases} 1.342\mu & \text{for Cvse (a)}, \\ 2.634\mu & \text{for Case (b)}. \end{cases}$$

These values are necessary to determine the effective relaxation lengths $\bar{L}_e$ for both cases, and also, these will be used in the calculation for the single-size or classical approximation. The results in the single size approximation are used for comparison with the present results to investigate the effect of the size distribution. The reference lengths $\bar{L}$, $\bar{L}_{max}$, and $\bar{L}_e$ can now be calculated from Eqs. (26-28), respectively, to yield

$$\bar{L} = 1.072 \times 10^{-2} m,$$

$$\bar{L}_{max} = 2.992 \times 10^{-1} m,$$

$$\bar{L}_e = \begin{cases} 5.336 \times 10^{-2} m & \text{for Case (a)}, \\ 1.633 \times 10^{-1} m & \text{for Case (b)}. \end{cases}$$
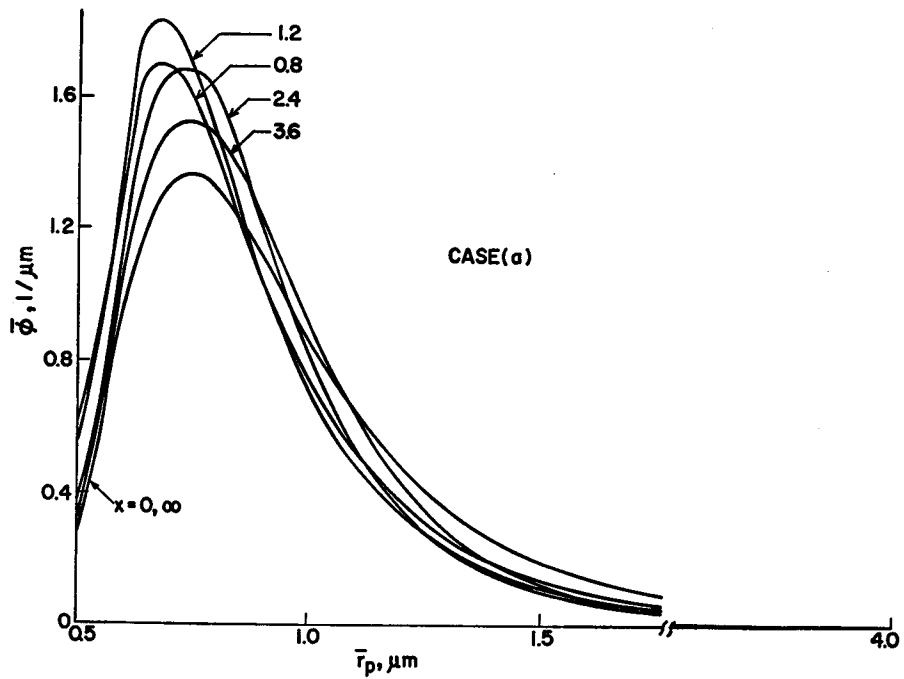
Fig.3.   Variation of distribution function ϕ for Case (a).
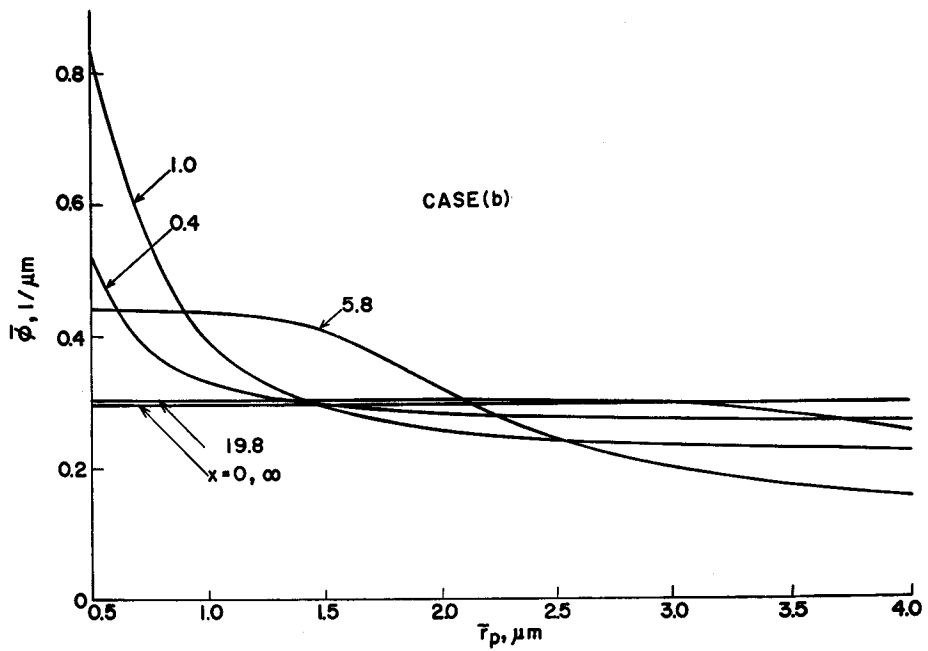
Fig. 4.   Variation of distribution function ϕ for Case (b).

These results clearly show that the particle radii r_p are far less than the relaxation lengths, which indicates the reasonableness of the assumptions introduced in specifying the boundary conditions for the particles in Eq. (34) or Eq. (29).

The variation of the distribution function along the distance x is shown in Fig. 3 for Case (a) and in Fig 4 for Case (b), where the numerical calculations have been carried out for $n=21$. Although, as was mentioned previously, the form of the distribution function in Case (a) is more realistic than that in Case (b), the result in Fig. (4) for Case (b) is more convenient for investigating the behavior of the particles in the relaxation region. In the early stage, after passing through the shock front, the cloud of particles with smaller sizes is compressed more effectively than that of particles with larger sizes. This results in an increase in the number of smaller sizes of particles, and then results in a decrease of the relative number of larger sizes of particles. Such a trend is most noticeable at about $x=1.0$ in Case (a). In the intermediate stage, however, the cloud of middle sizes of particles becomes gradually compressed, which results in a relative decrease in the number of smaller sizes of particles, and in a further decrease in the relative number of larger sizes of particles. The distribution function at $x=5.8$ shows such a situation. At a later stage, the cloud of larger sizes of particles becomes compressed appreciably, and then the relative number of larger sizes of particles begins to increase. The distribution function at $x=19.8$ demonstrates this situation. In the final stage at $x=+\infty$, the clouds of all sizes of particles become equally compressed and the distribution function has again its initial form.
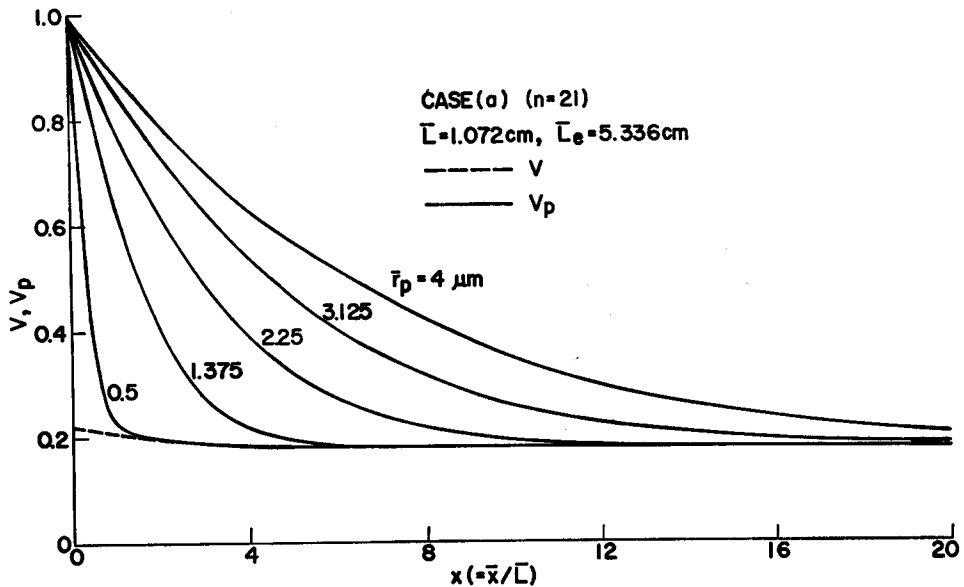

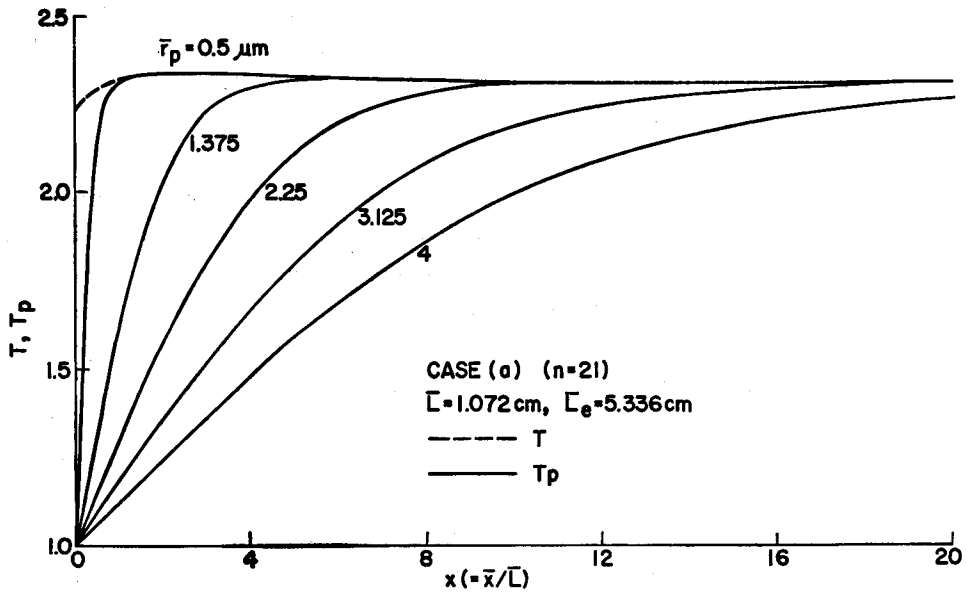Fig. 5. Variation of velocities along the distance x for Case (a).

Fig. 6.   Variation of temperatures along the distance x for Case (b).

Figs. 5 and 6 represent the variations of the velocity and the temperature along the distance x. For particles, only the results for several representative sizes of particles ($i=1$, 6, 11, and 21) are shown. The variations of the velocities are monotonous both for the gas and all sizes of particles, but those of the temperatures for the gas and smaller sizes of particles are not monotonous. A weak overshooting phenomenon is seen for these temperatures. Such a overshooting phenomenon is not found, in the results in Ref. 7, where three sizes of particles are considered. This may come from the appreciable differences between the drag coefficients, especially in the region near the shock front or in the region of the large particle Mach number, used in the numerical calculations.

The variations of the density, the pressure of the gas and also of the number density of the particles are shown in Fig. 7. This figure shows an appreciable difference between the results for Cases (a) and (b), which demonstrates the important role of the form of the distribution function in evaluating the effect on the flow behavior of the mixture of existing particles.

To compare the present results with those of the previous method where only a single size of particles is taken into account, sample calculations have also been carried out for the distribution function
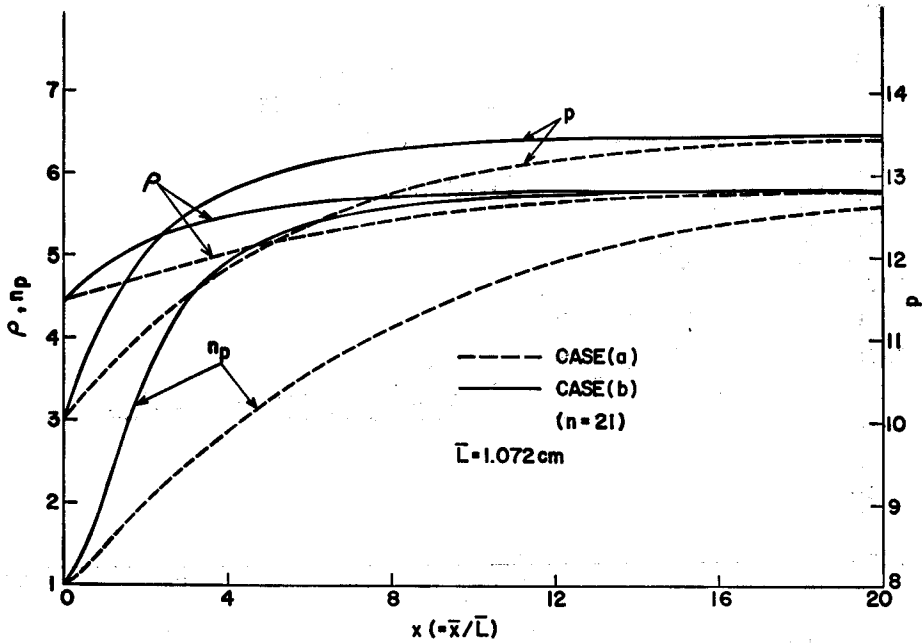
$$\phi_0 = \delta(r_p - \epsilon_p),$$

Fig. 7. Variation of p. ρ. and n_p along the distance x for Case (a) and Case (b).

where δ is Dirac's delta function. It will be easy to realize that in this case the basic equations (4-7) and (9-11) are reduced to the same as those for the single-size particles approximation. The numerical results for the gas velocity and temperature are shown in Figs. 8 and 9, with $\varepsilon_p = 1.342$ and 2.634 being compared with the results for Cases (a) and (b). These values of ε_p are the non-dimensional average or effective particle radii, $r_{pe} = \bar{l}_{p0}/\bar{r}_{pmin}$, for Cases (a) and (b), respectively.

For the gas velocity, the single-size approximation yields lower values when compared with the present results for Cases (a) and (b) in the whole relaxation region. For the gas temperature, the situation is a little more complicated. The former yields a higher value than the latter in the relatively small region near the shock front, but in the somewhat downstream region this situation is reversed.

As is easily anticipated theoretically, the width of the relaxation region for a single size of particles is always appreciably smaller than the present results. In many respects, the accuracy of a single size approximation is poor.

It would be important and interesting to compare the present results with those in Ref. 7, where three sizes of particles are considered. Unfortunately, this could not be done, because the particle drag coefficient and the Nusselt number (or f_p and g_p) used in the present calculations are appreciably different from those in Ref. 7, especially in the region near the shock front.
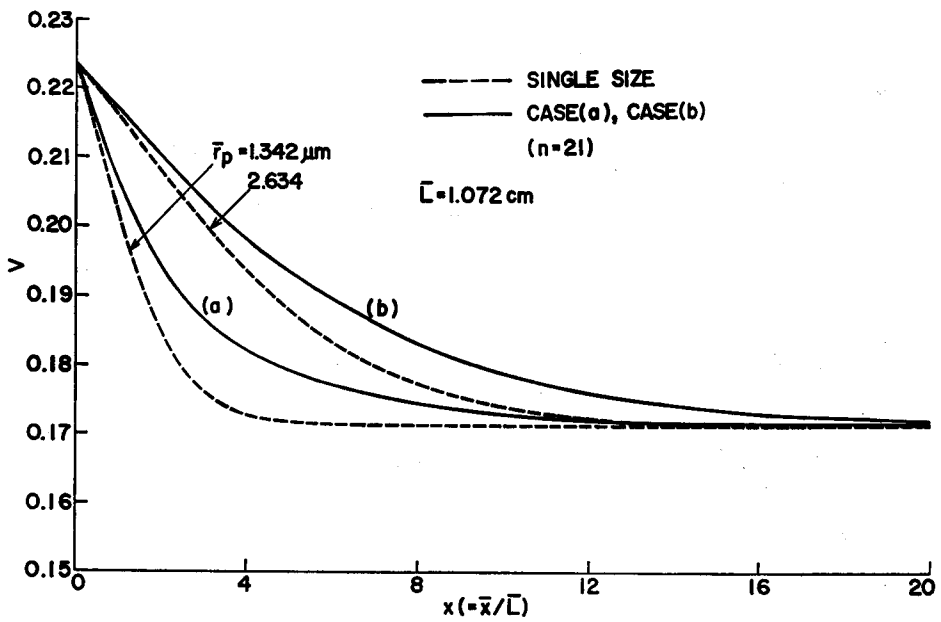
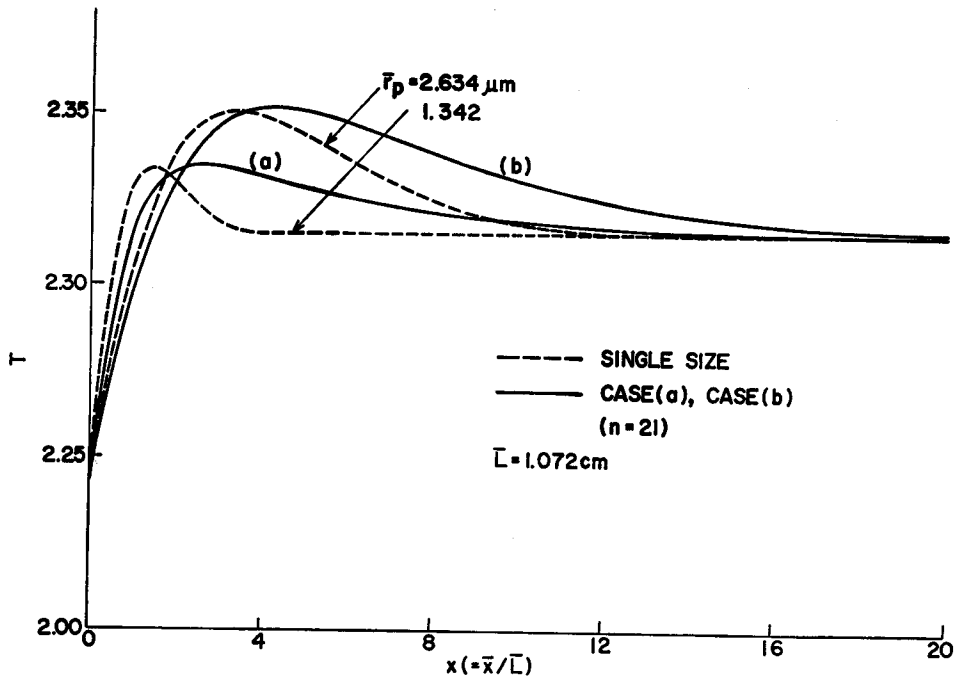Fig. 8. Comparison of velocities with those for single size of particles.

Fig. 9. Comparison of temperatures with those for single size of particles.

Concluding Remarks

The relaxation region behind a shock front of a dusty gas has been investigated in detail by taking into account a continuous distribution of particle sizes. It has been proved that the form of the particle distribution function has an appreciable effect on the gas velocity and temperature in the relaxation region. The usual approximation of single-size particles will lead to poor results in many practical cases. If attention is given only to the flow behavior of the gas, the assumption of a few sizes of particles may give a good approximation in some cases. Even in this case, however, the accuracy of the results will strongly depend on the actual from of the size-distribution of particles.

Practically, it is difficult to determine experimentally the form of the particle distribution function. When, however, a few sizes of approximation, as in Ref. 7, are applied, it is necessary to know the detailed form of the size distribution of particles in order to determine the few representative particle sizes and the corresponding number densities with sufficient reasonableness. Moreover, in the few sizes approximation, how to determine the few representative particle radii may not always be simple and easy, because the relaxation equations for particles strongly and complicatedly depend on the particle radii.

Appendix

The derivation of some of the basic equations will be given here. Firts, let us consider the continuity equation of particles with radii r_p in the range r_p to $r_p + dr_p$. Since the mass flow of these particles is constant along the distance x, we have

$$\left(\frac{4}{3}\pi\rho_{mp}\bar{r}_p^3\right)(\bar{n}_p\bar{\phi}dr_p)\,\bar{V}_p = \left(\frac{4}{3}\pi\rho_{mp}\bar{r}_p^3\right)(\bar{n}_{p0}\bar{\phi}_0 dr_p)\,\bar{V}_{p0},$$

which yields

$$\bar{n}_p\bar{\phi}\bar{V}_p = \bar{n}_{p0}\bar{\phi}_0\bar{V}_{p0},$$

or in the non-dimensional form

$$n_p\phi V_p = \phi_0. \qquad \text{(Eq. (8))} \tag{A1}$$

From this, we have

$$n_p\phi = \frac{\phi_0}{V_p}. \tag{A2}$$

Integrating (A2) over all sizes of particles yields

$$n_p\int_a^b\phi dr_p = \int_a^b\frac{\phi_0}{V_p}dr_p.$$

By using Eq. (19), it is given that

$$n_p = \int_a^b \frac{\phi_0}{V_p} dr_p. \qquad \text{(Eq. (9))} \qquad\qquad\qquad \text{(A3)}$$

Mathematically, it will be natural to consider that Eq. (A1) or Eq. (A2) is used to determine ϕ, and Eq. (A3) is used to determine n_p.

Next, consider the momentum equation of the mixture. Assuming that the volume fraction of the particles is negligible and that the particles exert no pressure, we can write the conservation of momentum as follows :

$$\rho \bar{V}^2 + \bar{p} + \int_{\bar{r}_{pmin}}^{\bar{r}_{pmax}} \left(\frac{4}{3}\pi\rho_{mp}\bar{r}_p^3\right)\bar{V}_p^2 (\bar{n}_p\bar{\phi} d\bar{r}_p)$$

$$= \rho_0\bar{V}_0^2 + \bar{p}_0 + \int_{\bar{r}_{pmin}}^{\bar{r}_{pmax}} \left(\frac{4}{3}\pi\rho_{mp}\bar{r}_p^3\right)\bar{V}_{p0}^2 (\bar{n}_{p0}\bar{\phi}_0 d\bar{r}_p).$$

This can easily be rewritten in the non-dimensional form as :

$$V + \frac{p}{\gamma M_0^2} + \nu\int_a^b \phi_0 V_p r_p^3 dr_p = 1 + \frac{1}{\gamma M_0^2} + \nu\int_a^b \phi_0 r_p^3 dr_p, \qquad \text{(Eq. (5))} \qquad \text{(A4)}$$

where use was made of the continuity equations (4) and (8) (or Eq. (A1)) for the gas and the particles, respectively. In a similar manner, the energy equation of the gas-parcle mixtture, Eq. (6), can easily be derived. From these discussions, it will be obvious that the present approach is microscopic.

References

1) Carrier. G, F., "Shock waves in a dusty gas," J. Fluid Mech. Vol. 3, 1958, pp. 531-545.
2) Schubert, B. S., "Existence and uniqueness of normal shock waves in gas-particle mixtures," J. Fluid Mech. Vol. 38, Part 3, 1969, pp. 633-655.
3) Rudinger, G. "Some Effects of Finite Particle Volume on the Dynamics of Gas-Particle Mixture," AIAA J. Vol. 3, No. 7, 1965, pp. 1217-1222.
4) Kliegel, J. R., "Gas Particle Nozzle Flows," Ninth International Symposium on Combustion, Academic Press, New York, 1963, pp. 811-826.
5) Buckley Jr., F. T., "Radiation-Resisted Shock Waves in Gas-Particle Flows," AIAA J. Vol. 9, No. 8, August, 1971, pp. 1603-1607.
6) Takano, A. and Hashima, T., "Normal Shock Waves in Gas-Particle Mixtures," J. A. S. M. Vo¹. 39, 1973, pp. 1553-1568, (in Japanese).
7) Marconi, F., Rudman, S. and Calia, V., "Numerical Study of One-Dimensional Unsteady Particle-Laden Flows with Shocks," AIAA J. Vol. 19, No. 10, October 1981, pp. 1294-1301.
8) Miura, H. and Glass, I. I., "On a Dusty-Gas Shock Tube," UTIAS Report No. 250, 1981.
9) Kliebel, A. R., "Analysis of Normal Shock Waves in Particle Laden Gas," Trans. of ASME, Journal of Basic Eng., Vol. 86, 1964, pp. 655-665.
10) Henderson, C. B., "Drag Coefficient of Spheres in Continuum and Rarefied Flows," AIAA J. Vol. 14, No, 6, June 1976, pp. 707-708.
11) Carlson, D. J. and Hoglund, R. F., "Particle Drag and Heat Transfer in Rocket Hozzles," AIAA J. Vol. 2, No. 11, Nov. 1980, pp. 1980-1984.